Bioorganic & Medicinal Chemistry Letters 26 (2016) 5657–5662

Contents lists available at ScienceDirect

Bioorganic & Medicinal Chemistry Letters

journal homepage: www.elsevier.com/locate/bmcl

Discovery of novel pyrrolidineoxy-substituted heteroaromatics as potent and selective PI3K delta inhibitors with improved physicochemical properties

Klemens Hoegenauer [a,*], Nicolas Soldermann [a], Christina Hebach [a], Gregory J. Hollingworth [a], Ian Lewis [a], Anette von Matt [a], Alexander B. Smith [a], Romain M. Wolf [a], Rainer Wilcken [a], Dorothea Haasen [c], Christoph Burkhart [b], Frédéric Zécri [a]

[a] Global Discovery Chemistry, Novartis Institutes for BioMedical Research, Novartis Campus, CH-4002 Basel, Switzerland
[b] Autoimmunity, Transplantation and Inflammation, Novartis Institutes for BioMedical Research, Novartis Campus, CH-4002 Basel, Switzerland
[c] Center for Proteomic Chemistry, Novartis Institutes for BioMedical Research, Novartis Campus, CH-4002 Basel, Switzerland

ARTICLE INFO

Article history:
Received 5 September 2016
Revised 20 October 2016
Accepted 23 October 2016
Available online 27 October 2016

Keywords:
Phosphoinositide-3-kinase delta inhibitor
PI3Kδ inhibitor
Structure-activity relationship
Physicochemical properties
Lipophilicity

ABSTRACT

In the recent years, PI3Kδ has emerged as a promising target for the treatment of B- and T-cell mediated inflammatory diseases. We present a cellular assay activity analysis for our previously reported 4,6-diaryl quinazoline PI3Kδ inhibitor series that suggests an optimal logP range between 2 and 3. We discovered novel analogues in this lipophilicity space that feature a chiral pyrrolidineoxy-group as a replacement for the position-4 aromatic ring of 4,6-diaryl quinazolines. These Fsp^3 enriched derivatives retain potency and selectivity towards PI3Kδ. Compared to 4,6-diaryl quinazolines, their permeability profile is improved and molecular weight as well as PSA are reduced. These modifications offer additional possibilities for derivative generation in a favorable physicochemical property space and thus increase the chances to identify a clinical candidate.

Phosphoinositide-3-kinase δ (PI3Kδ) is a lipid kinase expressed predominantly in hematopoietic cells and is composed of an enzymatic p110δ and a regulatory p85 subunit. PI3Kδ catalyzes the intracellular conversion of phosphatidylinositol 4,5-bisphosphate (PIP2) to phosphatidylinositol 3,4,5-trisphosphate (PIP3) downstream of a number of immune cell receptors (eg. BCR, TCR, FcεR1, CXCR5) [1–3]. Inhibition of PI3Kδ has been shown to be beneficial for the treatment of hematological malignancies such as CLL and iNHL [4–7]. Moreover, the PI3K/Akt pathway is activated in a number of autoimmune diseases such as rheumatoid arthritis (RA) [8] and systemic lupus erythematosus [9,10]. In patients with APDS (Activated PI3Kδ Syndrome), mutations in the PIK3CD gene encoding p110δ lead to an immunodeficiency characterized by recurrent infections and prominent lymphoproliferation [11–13]. In models of RA, PI3Kδ inhibitors have demonstrated efficacy with respect to inflammation and reduced bone and cartilage erosion. In allergic asthma, PI3Kδ has been shown to be overactive in neutrophils, T-cells, eosinophils, and B-cells [14]. Taken together, these data strongly indicate that PI3Kδ is a promising target for both inflammatory and autoimmune diseases [15–17]. As a consequence, a number of companies initiated efforts towards developing selective PI3Kδ inhibitors [18–26].

We have recently reported on the discovery of novel 4,6-diaryl quinazolines as PI3Kδ-selective inhibitors [27]. Representative quinazolines **1**–**3** (Fig. 1) are potent biochemical inhibitors of the PI3Kδ isoform with selectivity toward PI3Kα, PI3Kβ, and PI3Kγ (Table 1). This activity is also reflected in transfected Rat-1 cells stably overexpressing myristoylated, hence constitutively active, PI3Kα, β and δ isoforms ("cellular AKT phosphorylation assay"). This activity translates also in primary cellular assays such as inhibition of anti-IgM induced mCD86 expression on mouse splenocytes and inhibition of anti-IgM/IL-4 induced rCD86 expression in 50% rat blood.

While these 4,6-diaryl quinazolines offer an attractive activity profile, we also noticed some physicochemical property limitations for this series. Good physicochemical properties are required for oral drug candidates to ensure a) aqueous solubility to enable dissolution in the intestinal system, b) permeability to cross cellular barriers, and c) metabolic stability in order to achieve necessary exposure levels. 4,6-diaryl quinazoline **3**, one of our frontrunner compounds, illustrates that we were operating within borderline

* Corresponding author.
E-mail address: klemens.hoegenauer@novartis.com (K. Hoegenauer).

http://dx.doi.org/10.1016/j.bmcl.2016.10.069
0960-894X/

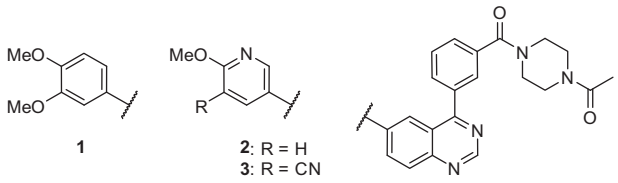

Fig. 1. 4,6-Diaryl quinazoline based PI3Kδ selective inhibitors.

ranges of some parameters that influence the ability of molecules to pass through cellular membranes. In particular, the high molecular weight (M = 492.5) and high polar surface area (PSA = 112) do not leave a lot of room for additional substitution and polarity without an increased likelihood of compromising absorption and permeability [28,29]. In order to identify general trends within that series, we thoroughly analyzed our dataset of 4,6-diaryl quinazolines. We sought to identify factors that would impact cellular activity, as we noticed quite some variation in IC_{50} ratios between the cellular AKT phosphorylation assay and the biochemical KGlo assay (Table 1, Fig. 2A, "shift bioch → cell") and also in IC_{50} ratios between the anti-IgM/IL-4 induced rCD86 expression in 50% rat blood and the cellular AKT phosphorylation assay (Table 1, Fig. 2B, "shift cell → blood"). For this analysis, we ensured that our dataset contained only biochemical IC_{50} values greater than 2.5 nM, the lowest truly measurable value considering an enzyme concentration of 5 nM in this assay. We found that both the assay shift bioch → cell as well as the assay shift cell → blood showed a trend to be logP dependent (Fig. 2A). In order to visualize the full data spread, the data is shown as box plots, nevertheless care needs to be taken in the interpretation of binned values [30]. In our view, the data suggested some trends that we could use to increase the likelihood of supportive physicochemical properties.

Regarding the assay shift bioch → cell, Fig. 2A illustrates that permeability to cross cellular membranes tends to decrease with lower lipophilicity. For logP values below 2, chances of a pronounced assay shift bioch → cell increase significantly. This is also reflected in Fig. 3 which shows that effective permeability ($logP_e$ at pH = 6.8) tends to decrease with lower lipophilicity. For compounds with logP < 3, effective permeability values below −6 become more frequent, increasing the risk of poor cellular activity and passive absorption. In contrast, an opposing trend with respect to lipophilicity is observed for the assay shift cell → blood (Fig. 2B), where higher logP values lead to an increased likelihood of higher assay shifts. We rationalized this observation with unspecific binding playing a more pronounced role in a whole blood assay that contains more plasma proteins and blood cells. From this analysis we concluded that the optimal 'lipophilicity target area' to ensure proper balance between cellular permeability and unspecific binding is the logP range between 2 and 3. This range has been termed the overall lipophilicity "sweet spot," which has been suggested as optimal for drug candidates [31]. From Fig. 3, it is also apparent that a PSA below 90 leads to better cellular permeability hence, our redesign also targeted replacing or omitting one of the two amide bonds in compounds **1**–**3**. Furthermore, it is generally desirable to increase the fraction of sp^3 carbon atoms (Fsp^3), as increasing the number of saturated carbon bonds has been associated with better properties and thus higher likelihood of success of advancing through the drug discovery pipeline [32,33]. As we were reaching the upper limit of the ideal molecular weight range with compounds **1**–**3**, an additional goal was to replace one of the aromatic rings rather than adding additional sp^3 rich elements on top of the existing scaffold.

As a result of the analyses discussed so far, we considered novel ways to improve on quinoxaline **5b**, an example for an alternative series with PI3Kδ selectivity that we pursued in parallel to

Table 1
Biochemical/cellular potency, PI3K isoform selectivity, and in vitro ADME parameters of PI3K inhibitors.

Cpd	Biochemical IC_{50} [μM][a]				Cellular IC_{50} [μM][a,c]			mCD86 IC_{50} [μM][a,d]	rCD86 IC_{50} [μM][a,e]	PAMPA $logP_e$[f]	HT-logP[g]	HT-sol[h]	PSA[i]	Shift bioch → cell[j]	Shift cell → blood[k]	Fsp^3[l]
	PI3Kα[b]	PI3Kβ[b]	PI3Kγ[b]	PI3Kδ[b]	PI3Kα	PI3Kβ	PI3Kδ									
1	0.127	1.94	0.220	0.009	1.32	3.38	0.039	0.034	0.035	−5.3	1.9	0.61	85	4	0.9	0.24
2	0.418	4.84	2.7	0.020	2.12	3.57	0.028	0.070	0.066	−5.1	2.7	0.80	89	1.4	2.3	0.19
3	0.262	1.65	4.63	0.007	3.44	6.53	0.049	0.074	0.072	−5.5	2.8	0.21	112	7	1.5	0.21
5a	3.23	>9.1	3.78	0.488	nd[m]	nd[m]	nd[m]	nd[m]	nd[m]	−3.8	3.7	0.08	74	nd[m]	nd[m]	0.35
5b	0.491	0.860	0.366	0.015	1.86	2.13	0.072	0.085	0.282	−3.8	3.8	0.04	74	5	4	0.35
7a	0.148	0.956	0.282	0.010	0.262	1.52	0.044	nd[m]	nd[m]	−4.8	5.3	0.009	83	4	nd[m]	0.40
7b	0.693	3.88	0.642	0.256	nd[m]	nd[m]	nd[m]	nd[m]	nd[m]	−4.4	4.9	0.006	83	nd[m]	nd[m]	0.40
9a	0.888	1.48	1.21	0.130	nd[m]	nd[m]	nd[m]	nd[m]	nd[m]	−3.5	3.6	>1.0	57	nd[m]	nd[m]	0.32
9b	0.842	1.94	2.07	0.110	nd[m]	nd[m]	nd[m]	nd[m]	nd[m]	−3.4	3.6	>1.0	57	nd[m]	nd[m]	0.32
10a	0.126	0.304	0.194	0.016	0.210	0.407	0.082	nd[m]	nd[m]	−3.9	2.6	>1.0	74	5	nd[m]	0.32
10b	0.676	1.79	1.23	0.146	nd[m]	nd[m]	nd[m]	nd[m]	nd[m]	−3.9	2.4	>1.0	74	nd[m]	nd[m]	0.32
12	0.218	0.669	0.698	0.009	1.03	1.78	0.028	0.082	0.297	−3.6	2.8	>1.0	77	3	11	0.33
13	0.386	0.360	0.978	0.005	1.38	1.28	0.079	nd[m]	nd[m]	−3.8	2.6	0.01	101	16	nd[m]	0.33
15	0.220	0.655	0.828	0.011	0.606	0.877	0.162	0.155	0.377	−3.7	3.4	>1.0	65	15	2.3	0.33
17	5.08	9.01	>9.10	0.188	>10.0	>10.0	2.84	nd[m]	nd[m]	nd[m]	2.8	0.37	77	13	nd[m]	0.33
19	0.424	1.03	2.94	0.022	2.36	3.21	0.646	nd[m]	nd[m]	−4.5	2.2	>1.0	77	29	nd[m]	0.33

[a] Mean of a minimum of two independent experiments; standard deviation for pIC_{50} values < 0.3.
[b] KGlo format.
[c] Inhibition of pAkt formation in Rat-1 cells.
[d] Inhibition of anti-IgM induced mCD86 expression on mouse splenocytes.
[e] inhibition of anti-IgM/IL-4 induced rCD86 expression in 50% rat blood.
[f] Effective permeability [10^{-6} cm s^{-1}] (pH = 6.8), n = 1.
[g] High-throughput logP measurement with immobilized artificial membranes, n = 1.
[h] High-throughput equilibrium solubility determination [mM] (pH = 6.8).
[i] Topological polar surface area.
[j] Shift biochemical → cellular IC_{50} for PI3Kδ, see Fig. 2A.
[k] Shift cellular IC_{50} → rCD86 (whole blood), see Fig. 2B.
[l] Number of sp^3 hybridized carbons/total carbon count.
[m] nd = not determined.